A quantitative conduction model for a low-resistance nonalloyed ohmic contact structure utilizing low-temperature-grown GaAs

Nien-Po Chen[a)]
Department of Physics, Purdue University, West Lafayette, Indiana 47907

H. J. Ueng, D. B. Janes, J. M. Woodall,[b)] and M. R. Melloch
School of Electrical and Computer Engineering, and NSF MRSEC for Technology Enabling Heterostructure Materials, Purdue University, West Lafayette, Indiana 47907

(Received 24 January 2000; accepted for publication 3 April 2000)

We present a quantitative conduction model for nonalloyed ohmic contacts to *n*-type GaAs (*n*:GaAs) which employ a surface layer of low-temperature-grown GaAs (LTG:GaAs). The energy band edge profile for the contact structure is calculated by solving Poisson's equation and invoking Fermi statistics using deep donor band and acceptor state parameters for the LTG:GaAs which are consistent with measured bulk and surface electrical properties of this material. The specific contact resistance is then calculated using an analytic expression for tunneling conduction through an equivalent uniformly doped Schottky barrier. The model has been used to fit measured specific contact resistances versus LTG:GaAs layer thickness and versus measurement temperature. These comparisons provide insights into the contact mechanism (electron tunneling between metal states and conduction band states in *n*:GaAs) and indicate that low barrier heights (0.3–0.5 V) and high activated donor densities ($\sim 1\times 10^{20}\,\mathrm{cm}^{-3}$) have been achieved in these *ex situ* contacts. © *2000 American Institute of Physics.* [S0021-8979(00)06413-6]

I. INTRODUCTION

Having ohmic contacts of low specific contact resistance, ρ_c, is always important for semiconductor device applications. As device dimensions shrink into the submicron and even nanometer scale, the issue of getting high quality contacts with low ρ_c is more demanding.

For semiconductor materials which have energy band gaps of about 1 eV or larger, tunneling based contacts are typically used.[1–3] Achieving low ρ_c in these contacts requires low barrier height Φ_B (corresponding to a relatively low work function metal and a low interface state density) and high activated doping density ($N_D - N_A$) for *n*-type contacts. In alloyed contact structures, the low interface state density and high activated doping density are achieved via diffusion from contact metal; this results in a metallurgical interface below the original semiconductor surface. Alloyed ohmic contacts to GaAs (Au–Ge–Ni for *n*-type GaAs and Au–Zn for *p*-type GaAs) are extensively used. Although low ρ_c ($<10^{-6}\,\Omega\,\mathrm{cm}^2$) can be achieved,[4] the rough interfaces and spatial nonuniformities from the alloying process are not suitable for nanometer scale devices or for applications which require planar interfaces.

Nonalloyed ohmic contacts can alleviate these problems, provided that suitable contact resistance can be achieved. With stoichiometric *n*-type GaAs (*n*:GaAs), low resistance contacts are problematic in *ex situ*, nonalloyed structures due to (i) midgap surface Fermi level pinning, which arises due to rapid oxidation of the surface and to the associated interface states, and (ii) the amphoteric behavior of Si, which limits the maximum activated donor density which can be achieved in the bulk. *In situ* nonalloyed contacts have been demonstrated with a ρ_c of mid-$10^{-7}\,\Omega\,\mathrm{cm}^2$ using Ag deposited on n^+ GaAs inside a molecular beam epitaxy (MBE) growth chamber,[5] which provides high ($N_D - N_A$) and low Φ_B. However, this approach has limited applications due to the *in situ* nature. Patkar *et al.*[6] demonstrated an *ex situ* nonalloyed contact to *n*:GaAs with ρ_c as low as $3\times 10^{-7}\,\Omega\,\mathrm{cm}^2$. In order to eliminate the problems associated with stoichiometric GaAs surfaces, the contact structure employs a thin cap layer (2–5 nm) of low-temperature-grown gallium arsenide (LTG:GaAs) on a heavily *n*-doped layer of GaAs (n^{++} GaAs). Low-resistance contacts can be realized after prolonged air exposure and photoresist processing, provided the contact metal (Ti/Au or Ag) is deposited within a short time period after the surface oxide layer is stripped. There have been a few device applications utilizing this *ex situ* nonalloyed ohmic contact technique, including shallow resonant tunneling diodes[7] and ohmic nano contacts.[8] A qualitative description of conduction through the contact has previously been presented[6] based on impurity band conduction through the states in LTG:GaAs and subsequent tunneling to the conduction band in n^{++} GaAs. The LTG:GaAs has a number of interesting electrical properties associated with the large density of point defects ($\sim 1\times 10^{20}\,\mathrm{cm}^{-3}$) arising from the excess As incorporated during growth.[9,10] Of particular interest, several studies[11–14] have addressed the electrical characteristics and chemical stability of LTG:GaAs surface layers. In order to provide an understanding of the conduction mechanism in this contact structure as well as a set of guide lines for achieving the best performance in com-

[a)]Electronic mail: npchen@physics.purdue.edu
[b)]Present address: Dept. of Electrical Engineering, Yale University, New Haven, CT 06520.

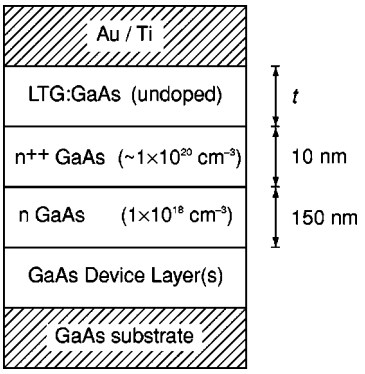

FIG. 1. Schematic of the device layer.

parable contacts, it is necessary to develop a quantitative model for the contact performance which incorporates parameters consistent with the various experimental observations.

In this article, we describe a physically based, quantitative model for the specific contact resistance of the LTG:GaAs nonalloyed contact structure. Experimental data for the specific contact resistance versus temperature are also presented. The model is used to predict the observed behavior of these data, along with that of published data for specific contact resistance versus LTG:GaAs layer thickness in order to verify the validity of the model and to determine the specific parameters of the samples developed to date. A discussion of the conduction mechanism and factors which determine the ρ_c of a given contact structure is also presented.

II. DESCRIPTION OF THE MODEL

Our model consists of a proper description of the states in the LTG:GaAs, a calculation of the energy band edge profile of the contact structure using a Poisson equation solver, and the specific contact resistance calculations. Since the calculated energy band edge profile can reasonably be approximated by a parabolic profile, analytical expressions for tunneling resistance through a uniformly doped Schottky barrier can be employed. This approach not only reduces the complexity of the analysis, but also allows us to understand the properties of the contact structure in terms of the Schottky barriers, which are well understood.

A. Layer description

The contact structure, shown in Fig. 1, consists of a Si-doped ($1\times10^{18}\,\mathrm{cm}^{-3}$) *n*:GaAs layer of 150 nm, a heavily Si-doped (nominally $1\times10^{20}\,\mathrm{cm}^{-3}$) n^{++} GaAs layer of 10 nm, and a thin cap of undoped LTG:GaAs layer of thickness *t* (typically 2–5 nm). The layers are grown by MBE on top of the GaAs substrate and the device layers. In this article, Ti (Ti/Au) metallization is studied, with the metal deposited *ex situ* and without an annealing process. The LTG:GaAs layer is grown at a temperature of ~250 °C and is not annealed, that is, the LTG:GaAs layer is in ''as-grown'' condition, with the excess As distributed primarily as point defects (antisite defects, along with Ga vacancies).

To simplify modeling of the contact structure without losing the physical picture, we focus on the top three layers—metal, LTG:GaAs, and n^{++} GaAs—and study their electrostatics. We will refer to this set of layers as the contact structure in the following. We identify the following quantities as the important parameters: the LTG:GaAs layer thickness *t*, the activated donor density $N(=N_D-N_A)$ in the n^{++} GaAs layer, the measurement temperature *T*, and the barrier height Φ_B (in volts) at the interface of LTG:GaAs and the metal.

B. Electronic properties of the contact structure

The electronic states in the undoped LTG:GaAs layer are described by the conduction and valence band parameters of stoichiometric GaAs, with the addition of a deep donor band and a shallow acceptor band to describe the states associated with excess As and Ga vacancies, respectively. From scanning tunneling microscopy (STM) spectroscopy on thick layers of undoped LTG:GaAs,[11,15] it was shown that there is a band of midgap defect states, whose energy is centered at 0.5 eV above the valence band edge E_v, and whose density is as high as $10^{20}\,\mathrm{cm}^{-3}$. Other studies show these defect states are donorlike[10] and attribute the states to arsenic antisite defects ($\mathrm{As_{Ga}}$), with characteristics differing from those of EL2,[16] likely due to the very high density. Optical absorption measurements on thick layers of undoped LTG:GaAs indicate that there is also a lower density ($\sim10^{19}\,\mathrm{cm}^{-3}$) of shallow acceptors,[17] which have been attributed to a gallium vacancy level $\mathrm{V_{Ga}}$.[18] For the model, we need a description of the electronic properties of these states, i.e., the densities $N_{T_{d,a}}$, energies $E_{T_{d,a}}$, and half widths $\Delta E_{T_{d,a}}$ of the energy distributions (assumed to be Gaussian) of these defect states, where subscript ''d'' refers to the deep donor band and subscript ''a'' to the acceptor band.

We have developed a set of parameters for the donor and acceptor states which is consistent with surface and bulk measurements of the electrical properties of ''as-grown'' LTG:GaAs. For the deep donor band, we use parameters consistent with experiment observations:[11,15,17] namely, $N_{T_d}=1\times10^{20}\,\mathrm{cm}^{-3}$, $E_{T_d}=E_v+0.5\,\mathrm{eV}$, and $\Delta E_{T_d}=0.25\,\mathrm{eV}$. Using a Poisson equation solver (ADEPT),[19] and incorporating the characteristics of the LTG:GaAs defect states, we calculate the energy band edge profile of a thick, uniform LTG:GaAs layer, along the device depth. Note that ADEPT uses Fermi statistics so that energy-dependent donor/acceptor ionization is accurately calculated. We adjust N_{T_a}, E_{T_a}, and ΔE_{T_a} to fit the bulk Fermi level position in undoped LTG:GaAs (approximately at 0.4 eV below E_c in the bulk), which has been observed experimentally.[20,21] The bulk Fermi level position corresponds to a condition where charge neutrality holds, i.e., one in which the density of ionized donors in the deep donor band compensates for the density of ionized acceptors, which is essentially equal to N_{T_a}. We find that $N_{T_a}=4.5\times10^{18}\,\mathrm{cm}^{-3}$, $E_{T_a}=E_v+0.1\,\mathrm{eV}$, and $\Delta E_{T_a}=0.2\,\mathrm{eV}$ yield the best fit.

In order to adequately model contact performance, it is essential to utilize parameters which are also consistent with the surface electrical properties of LTG:GaAs. Holden *et al.*[14,22] used reflection anisotropy spectroscopy (RAS) to

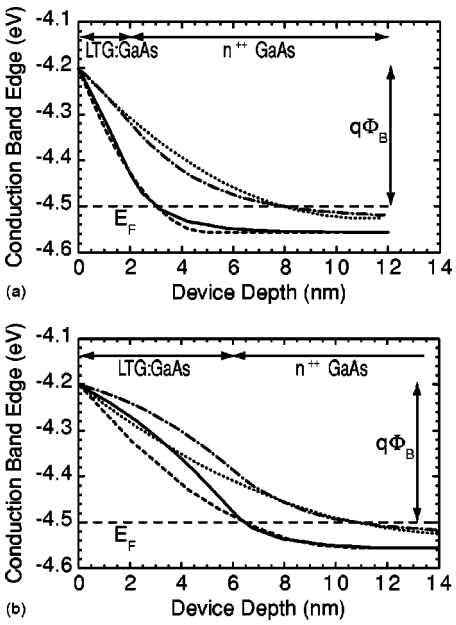

FIG. 2. Calculated energy band edge profiles of the contacts with t=(a) 2 and (b) 6 nm. Each subfigure shows two profiles simultaneously (dash-dotted and solid curves), corresponding to $N=10^{19}$ and 10^{20} cm^{-3}, respectively. The dotted and dashed curves represent the uniformly doped Schottky approximations to the respective profiles with the same barrier heights and effective donor densities.

study the near-surface electric field in a 500 nm thick undoped LTG:GaAs layer on top of a semi-insulating GaAs substrate. Due to the long air-exposure time (days), the surface Fermi level is pinned at midgap in this sample, consistent with observations of surface oxidation after 24 h of air exposure.[12] Using the electric field profile $\mathcal{E}(x)$ of the thick LTG:GaAs layer calculated by ADEPT with our LTG:GaAs model parameters and assuming midgap surface Fermi level pinning, we have calculated the relative RAS signal $\Delta R/R$ by numerically evaluating the integral of the weighted electric field along the layer depth, [Eq. (4b) of Ref. 22]. The calculated ratios between the $\Delta R/R$ for the LTG:GaAs sample and control samples [undoped GaAs and n:GaAs (Si: 1×10^{18} cm^{-3})] are 3.4:1:6.4, respectively. This is in good agreement with the reported measurement result of 2.9:1:6,[22] indicating that our description of the LTG:GaAs electronic properties is consistent with the measured effective near-surface electric field in this material.

For a thick LTG:GaAs layer, our model predicts a surface depletion thickness of approximately 20 nm, below which bulk Fermi level pinning occurs. Since the LTG:GaAs layer thickness in the typical contact structure is less than this depletion thickness, the surface depletion region in the contact structure will extend into the n^{++} GaAs layer. Note that we do not expect bulk Fermi level pinning within the LTG:GaAs layer of the contact structure, in contrast to a previous qualitative model.[6] The extension of the depletion region into the n^{++} GaAs layer is observed in the calculated energy band edge profile for the contact structure, which is shown in Fig. 2. The curves in Figs. 2(a) and 2(b) show the calculated conduction band edge profiles of contact structures with t=2 and 6 nm, respectively; each subfigure contains two profiles (dash-dotted and solid curves), corresponding to the structures with different activated doping densities in the n^{++} GaAs layer ($N=10^{19}$ and 10^{20} cm^{-3}), with all calculations at $T=300$ K and $\Phi_B=0.3$ V. The dotted and dashed curves in Fig. 2 correspond to profiles of equivalent uniformly doped Schottky barriers, as will be explained later.

For a given LTG:GaAs layer thickness, the structure with heavier doping in the n^{++} GaAs layer has a thinner depletion thickness and stronger electric field (the slope of the curve) in the depletion region. On the other hand, thicker LTG:GaAs layers yield thicker depletion thicknesses. The thicker LTG:GaAs layer also contains more negative charges, which results in a concave band profile in that region in Fig. 2. Since the majority of the space charge is in the n^{++} GaAs layer for the contact structures with thin LTG: GaAs layers (2–5 nm), the predicted energy band edge profile is relatively insensitive to the exact parameters of the defect states (N_T, E_T, and ΔE_T) for the structures used in the best contacts. Significant changes in these parameters will alter the range of t over which the uniformly doped Schottky approximation is valid, but will not change the general description of the contact.

C. Schottky approximation procedure

As is shown in Figs. 2(a) and 2(b), the calculated profile is approximated well for $t\sim$ 2–5 nm by the profile of a uniformly doped Schottky barrier, with the same Φ_B as the actual structure and an effective donor density N_{eff} determined by making the conduction band edge profile of the Schottky structure cross the Fermi level at the same device depth, x_F, as that of the profile for the contact structure. The conduction band edge profile of such a Schottky barrier is a parabola, assuming that all N_{eff} of the donors are ionized throughout the Schottky depletion region. We will denote this approximation barrier as the equivalent Schottky barrier. The advantage of the approximation is that we are able to utilize Schottky barrier tunneling resistance analysis, which is well established.[23–26] The ρ_c can then be calculated by using the expression for a uniformly doped Schottky barrier with Φ_B and N_{eff}. For relatively transparent barriers and/or low temperature, field emission (FE), i.e., tunneling at energies near the Fermi level, is the dominant electron transport mechanism. If the barrier is less transparent and/or the temperature is not as low, thermionic field emission (TFE) will be the dominant transport mechanism. For very thick barriers or high temperatures, thermionic emission (TE) will dominate. The formulas for the specific contact resistance of a Schottky barrier are derived by first considering the electron tunneling probability through the parabolic barrier, next calculating the tunneling current density, taking the derivative of the current density with respect to the applied bias, and finally evaluating its reciprocal at zero bias.[27,28] The formulas are

$$\rho_c = \begin{cases} \left(\frac{k}{qA^*T}\right) c_{\mathrm{FE}} \exp\left(\frac{q\Phi_{\mathrm{B}}}{E_{00}}\right), & \text{for } \frac{E_{00}}{kT} \gg 1 \text{ (FE)}, \\ \left(\frac{k}{qA^*T}\right) c_{\mathrm{TFE}} \exp\left(\frac{q\Phi_{\mathrm{B}}}{E_0}\right), & \text{for } \frac{E_{00}}{kT} \sim 1 \text{ (TFE)}, \\ \left(\frac{k}{qA^*T}\right) \exp\left(\frac{q\Phi_{\mathrm{B}}}{kT}\right), & \text{for } \frac{E_{00}}{kT} \ll 1 \text{ (TE)}, \end{cases} \tag{1}$$

with the characteristic energies defined as

$$E_{00} = \frac{qh}{4\pi}\sqrt{\frac{N_{\mathrm{eff}}}{\epsilon m^*}}, \tag{2}$$

$$E_0 = E_{00}\coth(E_{00}/kT), \tag{3}$$

and the coefficients c_{FE} and c_{TFE} are

$$c_{\mathrm{FE}} \equiv \left(\frac{\pi}{\sin(\pi bkT)} - \frac{\exp(-bu_{\mathrm{F}})}{bkT}\right)^{-1}, \tag{4}$$

$$c_{\mathrm{TFE}} \equiv \frac{kT}{\sqrt{\pi(q\Phi_{\mathrm{B}}+u_{\mathrm{F}})E_{00}}}\cosh\left(\frac{E_{00}}{kT}\right)\sqrt{\coth\left(\frac{E_{00}}{kT}\right)} \times \exp\left(\frac{u_{\mathrm{F}}}{E_0} - \frac{u_{\mathrm{F}}}{kT}\right), \tag{5}$$

with

$$b \equiv \frac{1}{2E_{00}}\ln\left(\frac{4q\Phi_{\mathrm{B}}}{u_{\mathrm{F}}}\right), \tag{6}$$

and q the electron charge magnitude, k the Boltzmann constant, h Plank's constant, ϵ the semiconductor permittivity, m^* the electron effective mass, $A^* = 4\pi qk^2m^*/h^3$ the effective Richardson constant, and u_{F} the Fermi level energy in the bulk (relative to the conduction band edge in the bulk).

To determine N_{eff} from the conduction band edge profile of the contact structure calculated with ADEPT, we set the equation,

$$u_{\mathrm{F}} = E_c(x_{\mathrm{F}}), \tag{7}$$

where $E_c(x)$ is the conduction band edge profile of a uniformly doped Schottky barrier and is defined as

$$E_c(x) = \frac{q^2N_{\mathrm{eff}}}{2\epsilon}(x-l)^2, \text{ for } 0 \leqslant x \leqslant l, \tag{8}$$

with l being the depletion depth

$$l = \sqrt{\frac{2\epsilon}{qN_{\mathrm{eff}}}V_{\mathrm{bi}}}, \tag{9}$$

and V_{bi} being the surface potential, which is equal to $(\Phi_{\mathrm{B}} + u_{\mathrm{F}}/q)$ at zero bias. Equation (7) yields

$$N_{\mathrm{eff}} = \frac{2\epsilon}{q^2x_{\mathrm{F}}^2}(\sqrt{q\Phi_{\mathrm{B}}+u_{\mathrm{F}}} - \sqrt{u_{\mathrm{F}}})^2. \tag{10}$$

The ratio N_{eff}/N varies between 0.6 and 0.02 for the cases considered in this article, with the smallest values corresponding to relatively large t. For small values of t, the observation that N_{eff}/N approaches a value of 0.5–0.6 (rather than 1) can be explained by considering the fraction of donors which are ionized in the two cases. The expressions for N_{eff} [Eqs. (8) and (10)] assume complete ionization, while the calculated profile for the contact structure utilizes Fermi statistics to calculate the fraction of the donors which is ionized. In order to make the values of u_{F} and N_{eff} in Eq. (10) self-consistent, it is necessary to iteratively (i) apply Eq. (10) and (ii) recalculate the Fermi level for a layer doped at N_{eff}. The initial value of u_{F} is from the conduction band edge profile of the contact structure, calculated with ADEPT. Since we are interested in heavily doped structures (large N), whose u_{F} does not change significantly with N (and N_{eff}), one iteration is sufficient to obtain reasonable consistency.

From the equivalent Schottky barrier parameters $(\Phi_{\mathrm{B}}, N_{\mathrm{eff}})$, E_{00} can be computed with Eq. (2). Then, we can choose the proper formula in Eq. (1) to calculate the specific contact resistance according to the electron transport regime indicated by the criteria. From the formulas it is apparent that the transport regime changes from TE, TFE, to FE when N_{eff} increases and/or T decreases.

A numerical example is given in the following. For a contact structure with $t = 2$ nm, $N = 10^{20}\,\mathrm{cm}^{-3}$, $\Phi_{\mathrm{B}} = 0.3$ V, and $T = 300$ K, the N_{eff} is found to be $2.0\times10^{19}\,\mathrm{cm}^{-3}$. Then, E_{00} is calculated to be 92 meV by Eq. (2) and E_{00}/kT to be 3.54. Since the latter is somewhat larger than unity, it is likely that the FE regime dominates, although this case is relatively close to the transition point between the FE and TFE regimes. Equation (1) yields $\rho_c = 4.2\times10^{-7}\,\Omega\,\mathrm{cm}^2$.

A more explicit condition for the validity of the FE regime in Schottky barriers is given by[23,27]

$$1 - bkT > \frac{kT}{\sqrt{2E_{00}u_{\mathrm{F}}}}, \tag{11}$$

which corresponds to the FE threshold of E_{00}/kT being in the range of 2.3–3.7 for the cases considered in this article. Note that Eq. (1) does not yield continuous ρ_c between FE and TFE regimes.[28] To obtain a smooth ρ_c transition, we utilize the following smoothing procedure in the transition region between the two regimes. We define ξ_0 as the value of E_{00}/kT at the FE to TFE crossover point and the half width (in E_{00}/kT) of the transition region as $\Delta\xi$.

$$\ln \rho_c = \begin{cases} \ln \rho_c^{(\mathrm{TFE})}, & \text{for } \dfrac{E_{00}}{kT} < \xi_0 - \Delta\xi, \\ \ln \rho_c^{(\mathrm{TFE})} + \dfrac{\ln \rho_c^{(\mathrm{FE})} - \ln \rho_c^{(\mathrm{TFE})}}{2\Delta\xi}\left(\dfrac{E_{00}}{kT} - (\xi_0 - \Delta\xi)\right), & \text{for } \left|\dfrac{E_{00}}{kT} - \xi_0\right| \leq \Delta\xi, \\ \ln \rho_c^{(\mathrm{FE})}, & \text{for } \dfrac{E_{00}}{kT} > \xi_0 + \Delta\xi. \end{cases} \tag{12}$$

That is, $\ln \rho_c$ is linearly interpolated between $\ln \rho_c^{(\mathrm{TFE})}$ and $\ln \rho_c^{(\mathrm{FE})}$ when E_{00}/kT is within $\xi_0 - \Delta\xi$ and $\xi_0 + \Delta\xi$. Linear interpolation on a logarithm scale is justified because ρ_c in Eq. (1) is exponentially dependent on E_{00}/kT. In our model, we use a fixed FE threshold ξ_0 and the smoothing procedure rather than Eq. (11).

III. PREDICTED SPECIFIC CONTACT RESISTANCE FROM THE MODEL

A. Specific contact resistance versus N and Φ_B

The calculated ρ_c as a function of N and Φ_B for a typical value of $t = 3$ nm at $T = 300$ K is plotted in Fig. 3. The operation regimes (FE and TFE) are also noted on the graph. Within the transition region between these regimes, the smoothing procedure described above has been applied, with $\xi_0 = 3$ and $\Delta\xi = 0.7$; the smoothed curve is shown as a thin solid line. The order of magnitude of ρ_c varies from 1 down to $10^{-7}\ \Omega\,\mathrm{cm}^2$ when N changes from 5×10^{18} to $1\times10^{20}\,\mathrm{cm}^{-3}$ and when Φ_B changes from 0.7 down to 0.3 V. Figure 3 also shows that the tunneling processes (FE and TFE) dominate for operation at room temperature. To have ρ_c as low as mid-$10^{-7}\,\Omega\,\mathrm{cm}^2$, N has to be as high as $10^{20}\,\mathrm{cm}^{-3}$ and Φ_B as low as 0.3 V. Figure 3 is useful to quickly estimate the range of parameter values which could fit a set of measured ρ_c data at room temperature.

B. Specific contact resistance versus LTG:GaAs layer thickness

Calculated values of ρ_c are plotted versus t for several values of N in Fig. 4. The calculation was performed with $\Phi_B = 0.3$ V and $T = 300$ K, using the same smoothing parameters employed in Fig. 3. On the same graph, measured data for ρ_c from two different sources are presented.[6,29] The measurements are made at room temperature, using the transmission line model (TLM) measurement technique,[30] on a series of contact structures with various LTG:GaAs layer growth thicknesses and nominal n^{++} GaAs layer doping density of $1\times10^{20}\,\mathrm{cm}^{-3}$. During the oxidation-stripping processes before metal deposition, about 2 nm of LTG:GaAs cap layer is removed. To account for the difference between the growth thickness and the actual thickness, we denote t_G as growth thickness and make the calculation in Fig. 4 using $t = t_G - 2$ nm. Note that the measured ρ_c increases with decreasing LTG:GaAs growth thickness for thickness less than 2 nm. Because of ineffective passivation, those devices with $t_G < 2$ nm will yield more oxidation on the surface and a corresponding increase in Φ_B due to large interface state density, resulting in higher ρ_c. Because of the change of Φ_B of these devices with $t_G < 2$ nm, their measured ρ_c can no longer be accurately described by the model with the original parameters.

For contact structures with $t_G > 2$ nm, we find that ($\Phi_B = 0.3$ V, $N = 5\times10^{19}\,\mathrm{cm}^{-3}$) and ($\Phi_B = 0.3$ V, $N = 1\times10^{20}\,\mathrm{cm}^{-3}$) can best fit the data of Patkar *et al.*[6] and of Morisette,[29] respectively. Note that $\Phi_B = 0.3$ V is required to fit the measured ρ_c. This is considerably lower than 0.7 V which would be expected if the surface Fermi level is pinned at midgap. This is consistent with experimental observation of surface stability of LTG:GaAs,[12,13] as will be discussed later. Therefore, our model can describe ρ_c successfully if

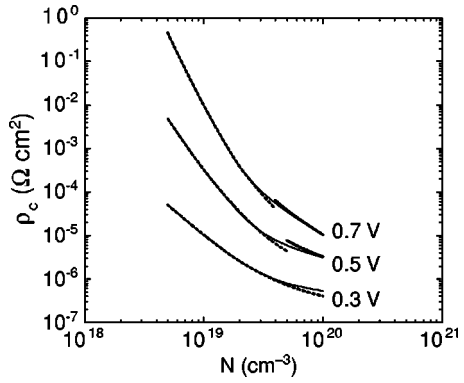

FIG. 3. Specific contact resistance as a function of n^{++} doping level (N) for T=300 K, t=3 nm, and barrier heights (Φ_B) of 0.3, 0.5, and 0.7 V. Dashed and solid curves indicate TFE and FE regimes, respectively; thin curves indicate the smoothed curves.

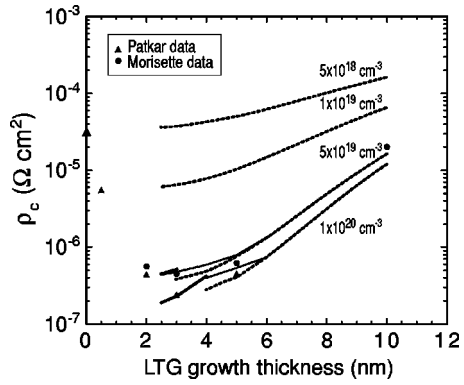

FIG. 4. Specific contact resistance as a function of LTG:GaAs growth thickness (t_G). Calculated values are shown for $T = 300$ K, $\Phi_B = 0.3$ V, and $N = 5\times10^{18}$, 1×10^{19}, 5×10^{19}, and $1\times10^{20}\,\mathrm{cm}^{-3}$. Dashed and solid curves indicate TFE and FE regimes, respectively; thin curves indicate the smoothed curves. Data from two experiments are also shown.

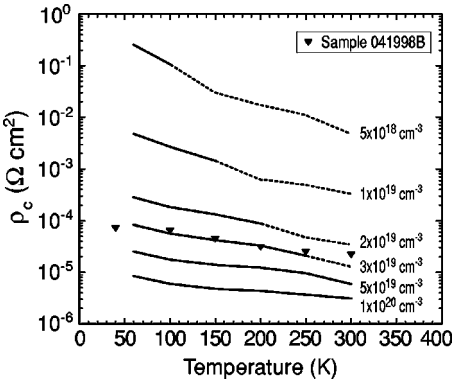

FIG. 5. Specific contact resistance as a function of temperature. Calculated values are shown for $t=3$ nm, $\Phi_B=0.5$ V, and $N=5\times10^{18}$, 1×10^{19}, 2×10^{19}, 3×10^{19}, 5×10^{19}, and 1×10^{20} cm^{-3}. Dashed and solid curves indicate TFE and FE regimes, respectively. The smoothing procedure is used with the same smoothing parameters as those in Figs. 3 and 4. An experiment data set is also shown.

the contact structure has t_G greater than 2 nm.

Also note that the fitting results of the model indicate that both Patkar *et al.* and Morisette's data have high values of N. That is, within the n^{++} GaAs layer depletion region close to the LTG:GaAs interface, the activated donor density (N_D-N_A) is well above the bulk limit of 5×10^{18} cm^{-3}. The significance of this result will be addressed in Sec. IV.

C. Specific contact resistance versus measurement temperature

In the calculation of ρ_c, several material properties are assumed to be independent of temperature for simple but accurate modeling, although they actually vary somewhat with T. They are the electron affinity of GaAs, the work function of the metal Ti, the activation energy of the dopant in n^{++} GaAs (Si), and the energy levels and half widths of the LTG:GaAs defect states. The calculated ρ_c as a function of T for various N, using $\Phi_B=0.5$ V and $t=3$ nm and using $t=t_G-2$ nm, are plotted in Fig. 5. On the same graph, a data set of ρ_c vs T measured using the TLM technique is presented for devices with $t_G=5$ nm and Ti/Au metallization. The Si doping density within the n^{++} layer is estimated to be 3×10^{19} cm^{-3} using the C-V profiling technique.[31] The measured ρ_c remains at a constant order of magnitude $(10^{-5}-10^{-4}\,\Omega\,\text{cm}^2)$ over the temperature range of 40–300 K.

We find that $\Phi_B=0.5$ V and $N=3\times10^{19}$ cm^{-3} fit the measurement data best. The model indicates that this contact operates in the FE regime over most of the temperature range. Although there are various possible fitting parameter sets of Φ_B and N which yield the same ρ_c as the measured one at a single temperature, only one (or ones in a narrow range) yields the best temperature dependence fit to the measurement, since the temperature dependences of ρ_c in the FE and TFE regimes are quite different. Take ρ_c measured at 300 K $(2.18\times10^{-5}\,\Omega\,\text{cm}^2)$ for example. From Fig. 3, such ρ_c can be obtained from $(\Phi_B,N)=\{(0.3\,\text{V}, 7.2\times10^{18}\,\text{cm}^{-3}), (0.5\,\text{V}, 2.4\times10^{19}\,\text{cm}^{-3}),$ and $(0.7\,\text{V}, 6.7\times10^{19}\,\text{cm}^{-3})\}$. Only $\Phi_B=0.5$ V and $N=2.4\times10^{19}$ cm^{-3} have the right temperature dependence as that of the measurement data. Further refinement yields the best fit to the data at 0.5 V, 3×10^{19} cm^{-3}. Due to the limited number of curves in Fig. 3, the best-fit parameters may not be exactly 0.5 V, 3×10^{19} cm^{-3}; nevertheless, this fit is very close to the exact fit. This analysis helps to eliminate a possible problem of having multiple fitting solutions and narrows down the range of the parameters. Most significantly, this comparison of temperature-dependent measurements and model calculation also helps to verify the conduction mechanism in our model.

IV. DISCUSSION

Comparison of the model prediction with experiment allows us to develop a quantitative description of the conduction mechanism of the contact structure. Based on this comparison, we conclude that the LTG:GaAs cap layer in the contact structure has two beneficial features to achieve low specific contact resistance: it allows a Φ_B which is significantly lower than 0.7 V (midgap) and it preserves the high space charge density layer in n^{++} GaAs.

The calculations were performed over the range of Φ_B (0.3–0.7 V) which could be expected for various process-related limits. The lowest barrier height corresponds to the case of minimal oxidation at the interface of the metal and the LTG:GaAs layer; its value is given by the difference of the work function of the deposited metal Ti (4.4 eV) and the electron affinity of LTG:GaAs, which is assumed to be the same as stoichiometric GaAs (4.1 eV).[25] The highest barrier height corresponds to the case of complete oxidation at the interface and the corresponding midgap pinning of the surface Fermi level. In order to fit the data from various experimental measurements, Φ_B values of 0.3–0.5 V are necessary. This implies that the surface Fermi level is not pinned at midgap. This is consistent with experiments where the LTG:GaAs surface is observed to oxidize slowly in air (time constant of hours) and remain electrically active.[12,13] Direct observations of this inhibited oxidation have involved freshly grown layers.[12,13] Since the semiconductor layers for the contacts have typically been exposed to air for days (or months) before processing, an oxide strip is necessary immediately before metal deposition. The realization of an interface with low Φ_B implies that the oxide-strip step can temporarily restore the surface to a state in which the Fermi level is not pinned at midgap, with a re-oxidation time constant expected to also be on the order of hours. The observed variation of Φ_B from sample to sample may be due to differences in the growth temperature of LTG:GaAs (and resulting changes in excess As), as well as to variations in processing.[29]

Si is the most widely used *n*-type dopant in MBE growth of GaAs since it allows the realization of relatively large activated donor densities, high mobilities in doped layers, and relatively small surface accumulation of dopant atoms, which enables the doping to be changed abruptly in superlattices and modulation doped structures.[32] In bulk *n*:GaAs, the net activated donor density (N_D-N_A) cannot go beyond 5×10^{18} cm^{-3} with Si as the dopant, due to the amphoteric nature of Si in this regime. During MBE growth, however,

the activated donor density near the surface of an n^{++} GaAs layer can reach as high as $10^{20}\,\mathrm{cm}^{-3}$, because the Fermi level is near midgap.[5,10] In structures with stoichiometric surface layers, this highly activated layer (<5 nm) oxidizes rapidly upon air exposure and is subsequently etched off in the oxide stripping process. In this structure, the chemical stability and surface Fermi level control provided by the LTG:GaAs maintain the high activated donor density in the portion of the space charge region immediately below the LTG:GaAs layer. Control of the Fermi level near the top of the n^{++} GaAs layer maintains the Si atoms primarily on donor sites during growth,[6] while the chemical stability of the LTG:GaAs cap layer prevents this interface layer from being oxidized (and etched away) upon air exposure. The comparison of experimental and predicted ρ_c in Figs. 4 and 5 indicates that values of $3\times10^{19}-1\times10^{20}\,\mathrm{cm}^{-3}$ have been achieved for (N_D-N_A) in this contact structure. The variability of N from sample to sample (in Figs. 4 and 5) is due in part to the types of sources used in various MBE systems and to the uncertainties in controlling the doping level in this regime. The LTG:GaAs provides both effective surface passivation and control of the Fermi level near the surface[11,12] and makes *ex situ* nonalloyed ohmic contacts possible.

The initial conduction model prescribed for this contact involved hopping or impurity band conduction through the midgap states in the LTG:GaAs and subsequent tunneling into the n^{++} GaAs. Based on the current model, which includes a more careful consideration of the electrostatics, we find that the deep donor (midgap) states in the LTG:GaAs layer are far below the Fermi level, so it does not appear that they directly participate in the conduction process. This conclusion is supported by the fact that ρ_c does not depend strongly on temperature, since both hopping-based contributions and conduction through a band far below the Fermi level would have relatively strong temperature dependences. Based on these observations, we can conclude that the major conduction mechanism in the contact is electron tunneling directly from the metal to the conduction band in the n^{++} GaAs layer, without hopping or band conduction through the defect states in the LTG:GaAs layer.

V. CONCLUSION

We have developed a quantitative conduction model for nonalloyed ohmic contacts to *n*:GaAs by considering this contact structure as an effective Schottky barrier. By incorporating deep donor and acceptor properties of LTG:GaAs which are consistent with the measured bulk and surface electrical properties of this material, we are able to construct a model in which the only fitting parameters are the barrier height and net activated donor density. The specific contact resistances calculated by the model are in good agreement with reported experiment data for ρ_c vs LTG:GaAs layer thickness and with our measurements of ρ_c versus temperature. We confirm that the conditions to have low specific contact resistance, namely (i) an activated donor density in the space charge region in n^{++} GaAs layer which is well above the bulk amphoteric limit, and (ii) low interface states and less oxidation at the metal–LTG:GaAs interface, are achieved by the LTG:GaAs cap layer. The dominant conduction mechanism is electron tunneling directly from the metal to the conduction band in the n^{++} GaAs layer.

ACKNOWLEDGMENTS

The authors would like to thank Professor S. Datta for inspiring discussions, Professor J. L. Gray for the helpful explanation of the ADEPT program, and Professor K. J. Webb, Takhee Lee, D. Morisette, and M. Hargis for informative communication.

[1] V. L. Rideout, Solid-State Electron. **18**, 541 (1975).
[2] Y. A. Gol'dberg, Semiconductors **28**, 935 (1994).
[3] A. G. Baca, F. Ren, J. C. Zolper, R. D. Briggs, and S. J. Pearton, Thin Solid Films **308–309**, 599 (1997).
[4] D. C. Look, *Electrical Characterization of GaAs Materials and Devices* (Wiley, Chichester, UK, 1989).
[5] P. D. Kirchner, T. N. Jackson, G. D. Pettit, and J. M. Woodall, Appl. Phys. Lett. **47**, 26 (1985).
[6] M. P. Patkar, T. P. Chin, J. M. Woodall, M. S. Lundstrom, and M. R. Melloch, Appl. Phys. Lett. **66**, 1412 (1995).
[7] H. J. Ueng, V. R. Kolagunta, D. B. Janes, K. J. Webb, D. T. McInturff, and M. R. Melloch, Appl. Phys. Lett. **71**, 2496 (1997).
[8] T. Lee *et al.*, Appl. Phys. Lett. **74**, 2869 (1999).
[9] M. R. Melloch, J. M. Woodall, E. S. Harmon, N. Otsuka, F. H. Pollak, D. D. Nolte, R. M. Feenstra, and M. A. Lutz, Annu. Rev. Mater. Sci. **25**, 547 (1995).
[10] M. R. Melloch, D. D. Nolte, J. M. Woodall, J. C. P. Chang, D. B. Janes, and E. S. Harmon, Crit. Rev. Solid State Mater. Sci. **21**, 189 (1996).
[11] S. Hong, R. Reifenberger, D. B. Janes, D. McInturff, and J. M. Woodall, Appl. Phys. Lett. **68**, 2258 (1996).
[12] T.-B. Ng, D. B. Janes, D. McInturff, and J. M. Woodall, Appl. Phys. Lett. **69**, 3551 (1996).
[13] D. B. Janes, S. Hong, V. R. Kolagunta, D. McInturff, T.-B. Ng, R. Reifenberger, S. D. West, and J. M. Woodall, Mater. Res. Soc. Symp. Proc. **448**, 3 (1997).
[14] T. Holden, W. D. Sun, F. H. Pollak, J. L. Freeouf, D. McInturff, and J. M. Woodall, Phys. Rev. B **58**, 7795 (1998).
[15] R. M. Feenstra, J. M. Woodall, and G. D. Pettit, Phys. Rev. Lett. **71**, 1176 (1993).
[16] D. C. Look, D. C. Walters, M. O. Manasreh, J. R. Sizelove, C. E. Stutz, and K. R. Evans, Phys. Rev. B **42**, 3578 (1990).
[17] D. C. Look, D. C. Walters, M. Mier, C. E. Stutz, and S. K. Brierley, Appl. Phys. Lett. **60**, 2900 (1992).
[18] J. Gebauer, R. Krause-Rehberg, and S. Eichler, Appl. Phys. Lett. **71**, 638 (1997).
[19] J. L. Gray, School of Electric and Computer Engineering, Purdue University, accessible at Purdue ECE Network Computing Hub ⟨http://www.ecn.purdue.edu/labs/punch⟩ (1995).
[20] A. C. Warren, J. M. Woodall, P. D. Kirchner, X. Yin, X. Guo, F. H. Pollak, and M. R. Melloch, J. Vac. Sci. Technol. B **10**, 1904 (1992).
[21] H. Shen, F. C. Rong, R. Lux, J. Pamulapati, M. Taysing-Lara, M. Dutta, E. H. Poindexter, L. Calderon, and Y. Lu, Appl. Phys. Lett. **61**, 1585 (1992).
[22] T. Holden, F. H. Pollak, J. L. Freeouf, D. McInturff, J. L. Gray, M. Lundstrom, and J. M. Woodall, Appl. Phys. Lett. **70**, 1107 (1997).
[23] F. A. Padovani and R. Stratton, Solid-State Electron. **9**, 695 (1966).
[24] C. R. Crowell and V. L. Rideout, Solid-State Electron. **12**, 89 (1969).
[25] S. M. Sze, *Physics of Semiconductor Devices*, 2nd ed. (Wiley, New York, 1981).
[26] E. H. Rhoderick and R. H. Williams, *Metal-Semiconductor Contacts* (Oxford University Press, New York, 1988).
[27] A. Y. C. Yu, Solid-State Electron. **13**, 239 (1970).
[28] K. Varahramyan and E. J. Verret, Solid-State Electron. **39**, 1601 (1996).
[29] D. Morisette, M.S. thesis, Purdue University, 1997.
[30] G. K. Reeves and H. B. Harrison, IEEE Electron Device Lett. **EDL-3**, 111 (1982).
[31] H. J. Ueng, N.-P. Chen, D. B. Janes, K. J. Webb, D. T. McInturff, and M. R. Melloch (unpublished).
[32] C. E. C. Wood, in *The Technology and Physics of Molecular Beam Epitaxy*, edited by E. H. C. Parker (Plenum, New York, 1985), pp. 61–82.